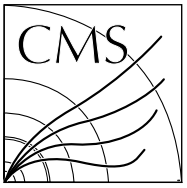

The Compact Muon Solenoid Experiment

CMS Note

Mailing address: CMS CERN, CH-1211 GENEVA 23, Switzerland

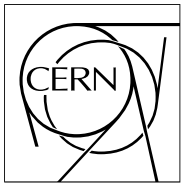

1 June 2006

Trilepton final state from neutralino-chargino production in mSUGRA.

W. de Boer, I.Gebauer, M. Niegel, C. Sander, M. Weber, V. Zhukov[*)b)]

IEKP, University Karlsruhe, Germany

K. Mazumdar

Tata Institute of Fundamental Research, Mumbai, India

Abstract

The direct production of neutralino-chargino $\chi_2^0\chi_1^\pm$ pairs in the mSUGRA scenario with decays into pure trilepton final states has a significant cross section for low neutralino masses. The trilepton signature was studied with the full and fast CMS detector simulations. The 5σ signal can be observed in the dilepton invariant mass distribution at the integrated luminosity of L_{int} $\geq$30 fb^{-1} for $m_{1/2} < 180$ GeV.

[*)] Valery.Joukov@cern.ch

[b)] On leave from SINP MSU

1 Introduction

The decays of neutralino χ_2^0 into an Opposite Sign Same Flavor (OSSF) lepton pair is one of the possible mSUGRA discovery signatures at the LHC. The neutralinos are abundantly produced in gluino and squark cascade decays with a multijet and large missing transverse energy final state. However for low neutralino masses, corresponding to low values of $m_{1/2} < 300$ GeV, the neutralinos can be produced directly, together with charginos: $pp \to \chi_2^0\chi_1^\pm$. This is a weak process and corresponds to the Standard Model (SM) reaction pp $\to$ WZ where the trilepton final state results from the leptonic decays. In case of SUSY the final state has in addition the lightest neutralino χ_1^0 and the trilepton appears either in three body decays of $\chi_2^0 \to \chi_1^0\ell^+\ell^-$ and $\chi_1^\pm \to \chi_1^0\ell^\pm\nu$ or in two body decays, $\chi_2^0 \to \ell\tilde{\ell} \to \ell\chi_1^0\ell$ and $\chi_1^\pm \to \ell\tilde{\nu} \to \ell\chi_1^0\nu$, $\chi_1^\pm \to \nu\tilde{\ell} \to \nu\chi_1^0\ell$.

The main signature of this reaction is two OSSF isolated leptons plus one of any flavor along with the absence of hard jets in the final state. The invariant mass of the OSSF dileptons exhibits a particular shape with the kinematic end point depending upon the event topology: either $M_{\ell\ell}^{max}$=$m_{\chi_2^0} - m_{\chi_1^0}$ for three body or
$M_{\ell\ell}^{max}$=$\sqrt{(m_{\chi_2^0}^2 - m_{\tilde{\ell}}^2)(m_{\tilde{\ell}}^2 - m_{\chi_1^0}^2)/m_{\tilde{\ell}}^2}$ for two body decays.

The trilepton channel has been intensively searched for at the Tevatron [1] with a negative result for $L_{int} \sim 300$ pb^{-1}. During the coming years the Tevatron will be able to investigate this channel with higher luminosity, thus probing the high cross section region at low $m_0, m_{1/2}$ further. The interest in the low $m_{1/2}$ and large m_0 region has been boosted by the recent observation, that the observed excess of diffuse Galactic gamma rays can be explained by the annihilation of the relic neutralino with $m_{\chi_1^0} < 100$ GeV/c^2 [2].

In this paper a study of the CMS discovery potential for the mSUGRA pure trilepton final state at the large m_0 and low value of $m_{1/2}$ is presented using full and fast detector simulation. In Section 2 the cross sections and event generation are discussed. Section 3 is dedicated to the detector simulation and event reconstruction framework. The event selection and background suppression is described in the Sections 4 and 5. Section 6 discusses the signal significance and the uncertainties. The CMS discovery reach for a luminosity of 30 fb^{-1} is presented in Section 7.

2 Cross sections and data samples

The signal and background cross sections were calculated with ISASUGRA 7.69 [4] and PYTHIA 6.225(CTEQ5L)[3] at leading order(LO). The NLO corrections have been taken into account by multiplying with the K factor. Full MC signal and background data samples for an integrated luminosity of $L_{int} = 30$ fb^{-1} have been generated with CMKIN 4.3.1 [5]. The detector performance was simulated with the full GEANT model (OSCAR 3.7.0+ORCA 8.7.3) and with the fast simulation (FAMOS 1.3.2) [5]. The low luminosity pile-up events have been added to the samples. Most of the data samples have been accessed or produced via GRID. In total $\sim 10^7$ events have been analyzed.

2.1 Signal

The neutralino-chargino mass spectrum and their production rates are defined in mSUGRA by the mass parameters m_0, $m_{1/2}$. The neutralino and chargino masses are approximately given by: $m_{\chi_1^0} \sim 0.4m_{1/2}$, $m_{\chi_2^0} \sim m_{\chi_1^\pm} \sim 0.8m_{1/2}$ and the production cross section $\sigma(\chi_2^0\chi_1^\pm) \propto m_{1/2}^{-4}$. Here only the $\chi_2^0\chi_1^\pm$ pairs were studied, the cross section for heavier neutralinos and charginos ($\chi_3^0, \chi_4^0, \chi_2^\pm$) is an order of magnitude smaller and was not considered.

For the trilepton final state the χ_2^0 and $\chi_1^\pm$ have been forced to decay to electrons or muons without any kinematic preselection. The decays into τ's produces soft leptons and would require a separate study. At relatively large m_0 >100 GeV and $m_{1/2}$ <300 GeV the neutralino χ_2^0 decays via off-shell Z* with subsequent decay into leptons (e, μ) with a typical branching Br($\chi_2^0 \to ll\chi_1^0$) $\sim$ 6%. The chargino $\chi_1^\pm$ decays to leptons with Br($\chi_1^\pm \to \ell\nu\chi_1^0$) $\sim 11\% \times 2$ via W*. The rest of decays is going into quarks. For two body decays, at $m_0 < 100$ GeV, the total branching ratio to leptons is Br($\chi_2^0 \to \ell\tilde{\ell} \to \ell\chi_1^0$) $\sim$ 10%. The rest of decays are mostly to staus. The neutralino with $m_{\chi_2^0} > m_{\chi_1^0} + m_h$ ($m_{1/2}$ >300 GeV) can decay into a light Higgs boson $\chi_2^0 \to \chi_1^0 h$, however the production cross section is small and this channel was not analyzed.

Figure 1 shows the trilepton cross section (LO) in the $m_0, m_{1/2}$ plane for tanβ= 10 and 50. The three body decays are dominant at low $m_{1/2} < 300$ GeV except for tan$\beta \leq 20$ and m_0 <150 GeV. The kinematic end point in the invariant mass is $M_{\ell\ell}^{max} \sim 0.42 * m_{1/2} - 18.4$ GeV/c^2 (for $m_0 \sim 1000$), thus moving into the Z-peak for $m_{1/2}$ >250 GeV. For larger $m_{1/2} > 300$ GeV after the Z-peak, the trilepton production cross section is below 1fb^{-1} and would require a large integrated luminosity. The m_0, $m_{1/2}$ plane is constrained for the low $m_{1/2}$ and

m_0 by the mass limits on the light Higgs boson ($m_h > 114.3$ GeV/c^2) and for low $m_{1/2}$ <150 GeV by the chargino mass limit ($m_{\chi_1^\pm} > 103$ GeV/c^2) from LEP [6]. The region excluded by the electroweak symmetry breaking (EWSB) requirements is indicated on Fig. 1 as well.

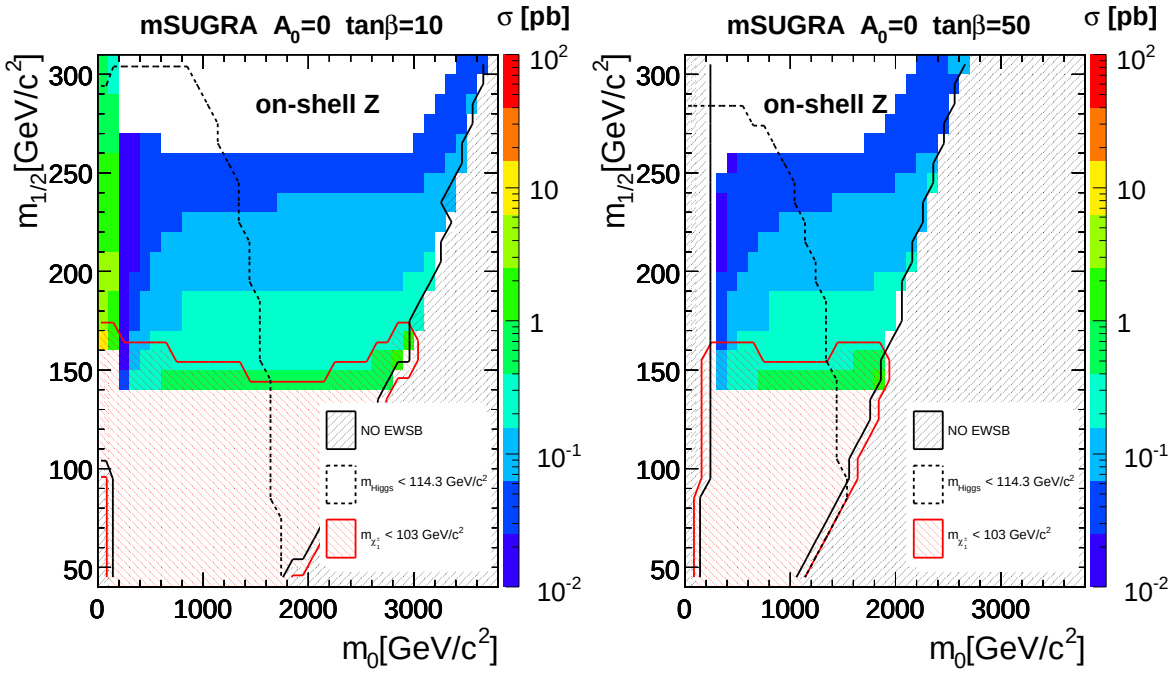

Figure 1: Trilepton cross section(LO) from direct neutralino-chargino production for two values of tanβ=10(left) and 50(right).

Table 1: Trilepton cross sections for the CMS test points

	$m_{1/2}$ [GeV/c^2]	m_0 [GeV/c^2]	tanβ	σ_{tot}^{LO} [pb]	$\sigma^{LO} \times BR3l(e,\mu)$ [pb]	$\sigma^{NLO} \times BR3l(e,\mu)$ [pb]	M_{ll}^{max} [GeV/c^2]
LM1	250	60	10	42	0.062	0.088	81
LM2	350	175	35	7.3	$1.8\ 10^{-4}$	$2.2\ 10^{-4}$	-
LM3	240	330	20	3.1	0.0094	0.012	82.3
LM4	285	210	10	18.8	0.009	0.012	91.2 (Z)
LM5	360	230	10	6.0	$0.8\ 10^{-3}$	$1.0\ 10^{-3}$	91.2 (Z)
LM6	400	85	10	4.0	0.022	0.028	76.7
LM7	230	3000	10	8.4	0.039	0.051	55.3
LM8	300	500	10	8.9	0.008	0.01	91.2 (Z)
LM9	175	1450	50	24.6	0.095	0.125	52.2

Table 1 presents cross sections for the Low Mass (LM) CMS test points and values for the kinematic end point of the dilepton invariant mass $M_{\ell\ell}$. The NLO K factor was calculated with PROSPINO [7] and is decreasing from 1.30 at $m_{\chi_2^0} = 150$ GeV/c^2 to 1.25 at $m_{\chi_2^0} = 300$ GeV/c^2. The trilepton signal has non negligible cross section for the LM9, LM7, LM3 (three body) and the LM1, LM6 (two body) points. For the LM4, LM5 and LM8 the neutralino decays via on-shell Z and cannot be distinguished from the background or decays at LM5 dominantly to the light Higgs boson h_0. For LM2 the neutralinos and charginos decay mostly into staus and h_0. Figure 2 shows the expected invariant mass of the OSSF leptons for different points at $L_{int} = 30$ fb^{-1}. The OSSF leptons were required to be inside the acceptance of $|\eta| < 2.4$ and to have a transverse momentum of $P_T > 3(5)$GeV/c for muons(electrons) pairs. The LM9 point has the largest cross section and was used as a reference in this analysis (called signal thereafter), for the 30fb^{-1} ~3700 events are produced. The selection criteria have been tuned to this point, the 2 body region at low m_0 may require another optimization. The LM9 data sample was generated using both, full and fast simulations. Other test points and the SUSY scan over the m_0, $m_{1/2}$ plane have been done with

the fast simulation.

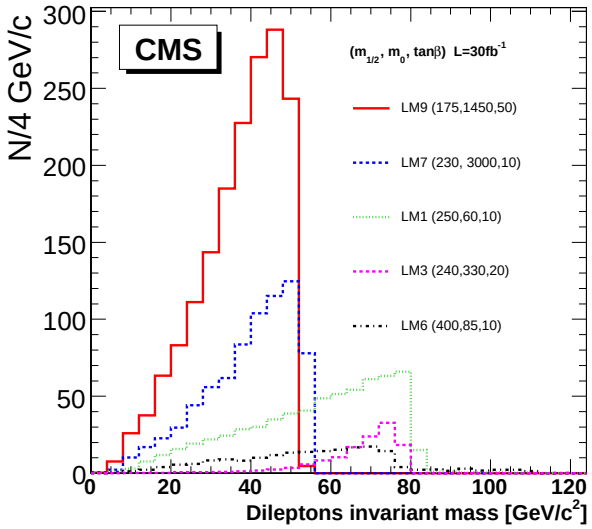

Figure 2: Invariant mass of OSSF leptons from χ_2^0 decay at generator level for different benchmark points at $L_{int} = 30$ fb^{-1}.

2.2 Backgrounds

Any reaction which can produce the OSSF lepton pair with sufficiently high P_T can be a potential background for the trilepton final state. The background channels can be divided into a few groups:

- Direct production of vector bosons ZW and ZZ with leptonic decay of Z and W bosons. These channels can be suppressed by excluding the Z boson invariant mass for the OSSF leptons.
- $t\bar{t}$, Wt+jets , WW+jets channels. The OSSF leptons originate from different decays and the third lepton appears from a jet not vetoed by the jet veto and having either an isolated lepton or a large electromagnetic component. A central jet veto removes part of these backgrounds.
- SUSY background is coming from the cascade decays where leptons are not produced by the neutralino decays and the particular shape of the invariant mass distribution is lost. Moreover the trilepton from the direct neutralino-chargino production can be contaminated with the neutralino produced after squarks and sgluino decays in association with jets. Such events, passing the selection, can enhance the signal. The SUSY background depends upon mSUGRA parameters. In this study the inclusive mSUGRA channel for the LM9 point except the direct neutralino-chargino production have been considered as the SUSY background.
- Drell Yan(DY), Z+jets and $Zb\bar{b}$ produces a high P_T OSSF lepton pair from Z or gamma decays. The Z+jets are acquiring the third lepton from jets. For the DY the third lepton is coming from the jets produced from the initial state radiation (ISR) gluon splitting into the $q\bar{q}$ pair. Most isolated leptons($\sim 75\%$) are produced from $b\bar{b}$ with $b \to l + jets$. The lepton's isolation and the veto on the Z peak reduce part of this background but due to large cross sections ($\sigma_{Z+jets,DY} \sim 10$ nb) , the DY and Z+jets channels can be the most important. Since it is difficult to simulate the full samples, a generator level preselection is required.
- W+jets and QCD channels intrinsically have only one or no isolated leptons. However the missing leptons can be produced by jets. The large cross section prevents the detailed analysis of these channels. In this study only estimations are presented.

The background cross sections have been calculated at LO with PYTHIA plus TopReX($t\bar{t}$, Wt)[8] or ALPGEN($Zb\bar{b}$)[9] and corrected to NLO with the K factors. For all backgrounds the Z and W bosons were forced to decay leptonically to e, μ and $\tau \to e, \mu$. No kinematic cuts have been used except for the Z+jets, DY and $Zb\bar{b}$, where three

leptons were preselected at the generator level to have P_T >5 GeV/c and $|\eta|$ <2.4. The effect of this preselection is discussed. Full data sample corresponding to $L_{int} = 30$ fb^{-1} have been simulated with the fast simulation veryfied with the smaller samples ($\sim 10^4$) produced in full simulation. A summary of the background cross sections and used statistics is presented in Table 2.

After reconstruction fake leptons can appear which can increase both, the number of background channels and, in case of preselections, number of background events in each channel. The detailed study of fakes would require simulation of large data samples in full simulation and is beyond of the scope of the current paper. The contribution of fakes is evaluated from the fast simulations. On the other hand the fake rates depend on the simulation model and the reconstruction algorithms which are expected to be significantly improved after beginning of the LHC operation and the estimation can be considered as an upper limit.

Table 2: Background $\sigma \times Br$ and list of data samples used in the analysis.

channel	$\sigma \times Br(e,\mu,\tau)$ [pb]	Nev, 30fb^{-1}	Full sim.	Fast sim.
ZW	1.68^{NLO}	5 10^4	5. 10^4	2. 10^5
ZZ	0.16^{NLO}	4800	10^4	2. 10^5
$t\bar{t}$	88^{NLO}	2.6 10^6	3. 10^5	2.6 10^6
Wt+ jets	10^{NLO}	3 10^5	1. 10^5	1. 10^6
SUSY(LM9)	13.1^{NLO}	4 10^5	10^4	5. 10^5
WW+jets	19.8^{LO}	6 10^5	10^4	4. 10^5
$Zb\bar{b}$ (3lept.)	2.8^{LO}	8.4 10^4	-	7.1 10^4
Z+jets (3lept.)	15.4^{LO}	4.6 10^5	10^4	9.2 10^5
DY (3lept.)	15.1^{LO}	4.5 10^5	10^4	8.5 10^5
W+jets($>30GeV/c$)	1.8 10^4 ^{LO}	5.4 10^8	10^5	5 10^5
QCD($>50GeV/c$)	2.4 10^7 ^{LO}	7.4 10^{11}	5 10^4	10^6

3 Event reconstruction

The simulated signal and background events have been reconstructed with the official CMS software [5] using the same analysis code and reconstruction algorithms.

3.1 Trigger

All events have been required to pass first level (L1) and high level (HLT) triggers. Table 3 shows how the trilepton signal events (LM9) are distributed among different L1 streams before and after offline selection, which will be discussed in the following sections. The streams population was calculated as the number of events in the stream divided on the total number of events passed a global L1 trigger.

The dimuons and the single muons are the main L1 trigger channels where the trilepton state is expected. The single electron and dielectrons streams are less populated due to higher thresholds. Some of the electrons can also be identified as τs, populating the τ streams. The increase of the muons channels after offline selection is due to the higher threshold used in the offline selection.

The distribution of the LM9 signal in HLT channels before and after offline selection is presented in Table 4. The HLT algorithms can be optimized even during CMS operation and the presented results are indicative.

The cumulative dimuon and dielectron streams trigger efficiency for the LM9 is 86% at L1 trigger and 91% at HLT, yielding a total efficiency of 78%. More details about the trigger efficiencies for the signal and backgrounds are presented in Table 6.

The trigger efficiency depends on the kinematics of the leptons which in turn depends on the mSUGRA parameters. The efficiency for the mSUGRA trileptons in the m_0, $m_{1/2}$ plane is presented in Figure 3. The scan was produced in fast simulation. The trigger selection cuts have been applied to the objects reconstructed using offline algorithms and the overall trigger efficiency was normalized to the one obtained from the full simulation at LM9 test point. For the large $m_{1/2}$ values the produced leptons are harder and the trigger efficiency is increasing, partially compensating a decrease in the cross section.

Table 3: L1 inclusive trigger streams for the LM9 mSUGRA point before and after offline selection.

L1 stream	threshold(LL) GeV/c(GeV)	% before selection	% offline selected
single μ	14	64	90
2 μ	3	41	74
single e/γ	20	50	45
2 e/γ	17	29	25
$\mu + e/\gamma$	5+15	30	48
$\mu + jet$	5+30	5	1.0
$\mu + \tau$	5+25	21	34
$\mu + MET$	5+45	10.5	17
$e/\gamma + \tau$	14+52	12	11
$\tau + MET$	35+40	16.5	20

Table 4: HLT streams for the LM9 point before and after offline selection.

HLT stream	threshold(LL) GeV/c	%	% offline selected
single e	26	41	38
2 e	14.5	24	24
single μ	19	56	82
2 μ	7	37	70
$e + \tau$	16+52	8	5
$\mu + \tau$	15+40	7.5	13

3.2 Leptons

The leptons in this analysis are used for the event selection and reconstruction of invariant masses. In CMS the muon reconstruction efficiency depends on the P_T^{μ} and is above 80% for P_T >5 GeV/c. The combined muon momentum resolution in the CMS Muon System plus Tracker is $\leq 1.5\%$ for these energies. For electrons the reconstruction efficiency is defined by the ECAL thresholds and amounts to ∼80% at $E^e > 10$ GeV. The electron momentum resolution using the combined Tracker and ECAL measurements is $\leq 3.5\%$ for $E^e > 10$ GeV.

The muons have been reconstructed in full and fast simulations with similar methods [5]. The muon track in muon stations was fitted using a Kalman-filter and extrapolated to the inner silicon tracker. The isolation of the reconstructed muons has been done in the cone $\Delta R = \sqrt{\Delta\eta^2 + \Delta\phi^2} < 0.3$; the sum of the transverse track momenta ($P_T^{track} > 0.8$ GeV/c) in this cone has to be less than 1.5 GeV/c and the sum of the transverse energy deposition in the calorimeter has to be less than 5 GeV. In order to avoid ghost tracks the OSSF muons with $\Delta R < 0.2$ have been rejected. In Figure 4 the P_T distribution of the MC tagged muon from the $\chi_1^{\pm}$ decay is plotted at generator level and after reconstruction with full or fast simulations. The reconstruction efficiency of such muons with $P_T^{\mu} > 5$ GeV/c and η <2.4 is listed in Table 5 for the events accepted by the trigger. The P_T distributions of muons ordered by P_T are shown in Figure 5 for the signal and important backgrounds. A small peak for the background channels at low P_T for the highest P_T muons corresponds to the single muon events, like $2e + \mu$. From Figure 5 it is clear that the first two highest P_T muons can be selected with the trigger cuts (> 7 GeV/c) but in order to suppress backgrounds the third muon should be also hard (> 10 GeV/c).

The electrons were reconstructed using information from the Tracker matched with the Calorimeters energy deposition. For the final electron identification the Electron Likelihood method [10] was used where different variables like E/P(super-cluster energy/ track momentum), $\frac{E_{HCAL}}{E_{ECAL}}$ (fraction of the HCAL and ECAL energy depositions), $E_{3\times3}/E_{5\times5}$(ratio of energy in 3×3 and 5×5 ECAL crystals) , $\Delta\eta = |\eta_{sc} - \eta_{track}|$ (difference between super-cluster and track position), $\sigma_{\eta\eta}$ (shower spread in longitudinal direction) are combined in one likelihood function $eleId$. The electron was selected if the value was $eleId > 0.65$. The electron was isolated by the requirement of tracks $\sum P_T$ <1.5 GeV/c in a cone $\Delta R < 0.3$ similar to the muons. Some muons from DY with final state photon radiation can be misidentified as an electron. These fake electrons have been removed by matching the electron track with the reconstructed muons in $\Delta R < 0.2$. The P_T distribution of electrons from the $\chi_1^{\pm}$ decay tagged by MC is shown in Figure 4. A summary of the electron identification efficiencies is presented in Table 5. The P_T distributions of electrons and muons ordered by P_T are shown in Figure 5(right) for the signal and backgrounds. Again, as for the muons, the lowest P_T electron is important for the background rejection.

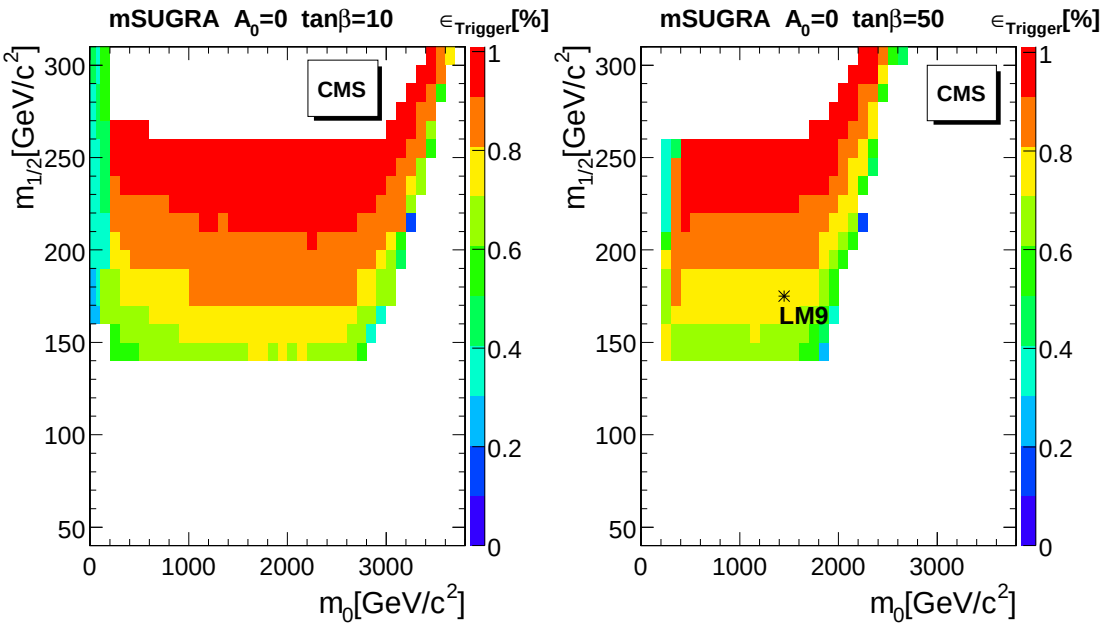

Figure 3: Trigger efficiency (L1+HLT) in mSUGRA m_0, $m_{1/2}$ plane for tanβ=10(left) and 50(right).

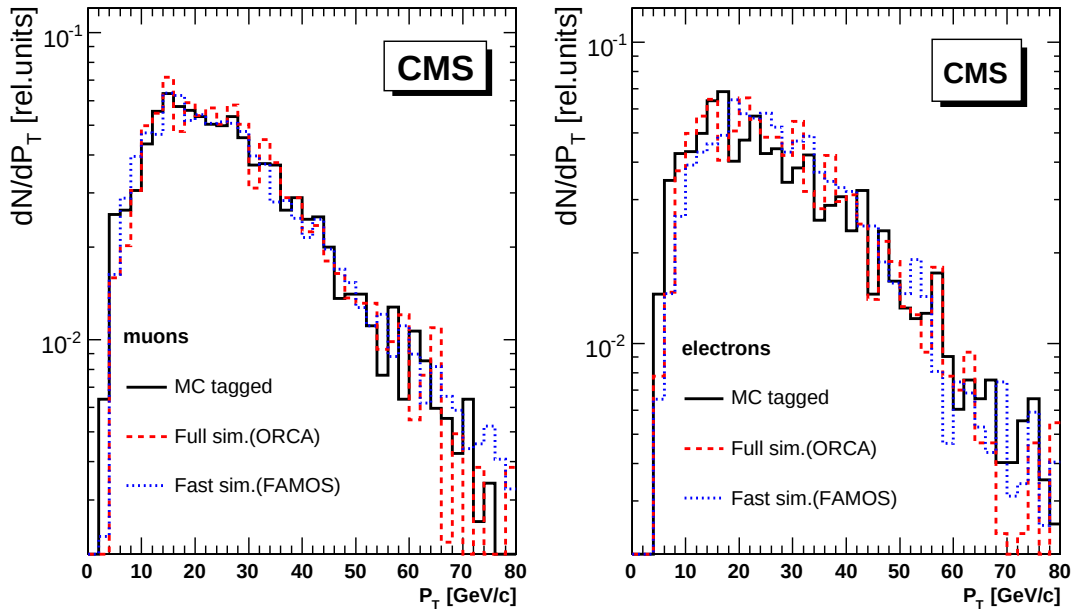

Figure 4: Left: Normalized P_T distribution of the generated and reconstructed muons from the $\chi_1^{\pm}$ decay in full(ORCA) and fast(FAMOS) simulations. Right: The P_T distribution of the generated and reconstructed electrons from the $\chi_1^{\pm}$ decay.

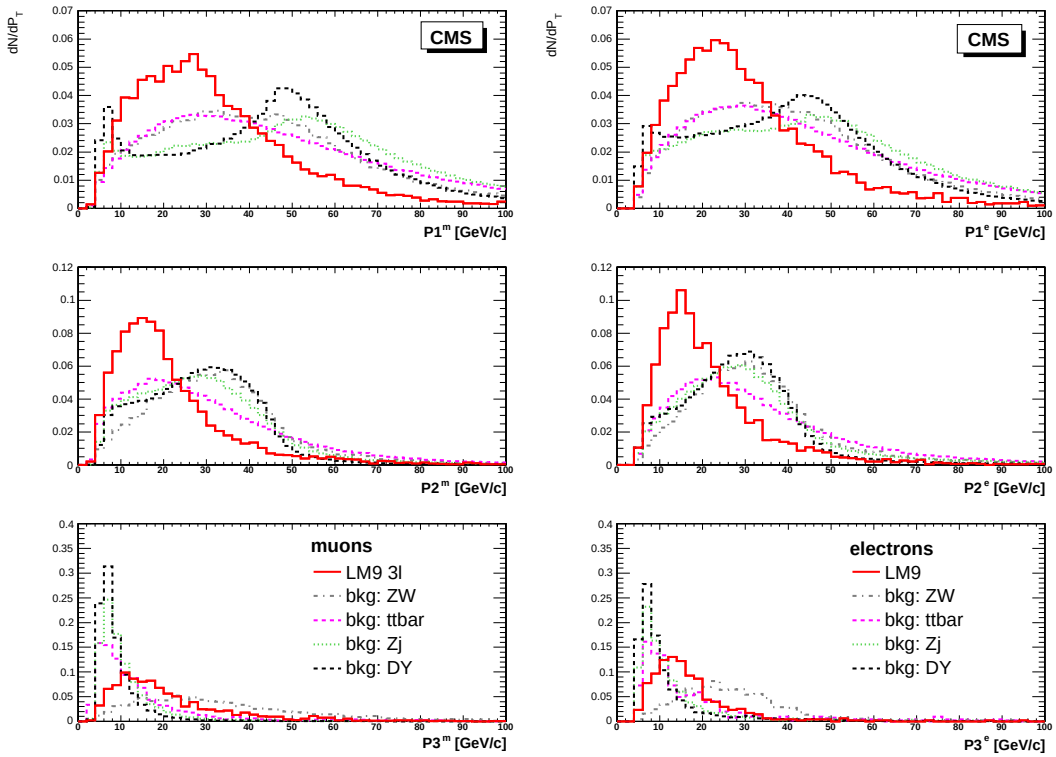

Figure 5: Normalized P_T distributions of the muons (left) and electrons (right) for the signal (LM9) and backgrounds, ordered by P_T.

Table 5: Lepton reconstruction efficiencies for the signal in ORCA and FAMOS.

	Full (ORCA)	Fast (FAMOS)
muons ($P_T > 5$ GeV/c)		
reconstruction efficiency, %	96	97.5
efficiency after isolation , %	78	83
electrons ($P_T > 10$ GeV/c)		
reconstruction efficiency , %	88	85
efficiency after isolation, %	66	61

3.3 Jets

The central jets with $|\eta|$ <2.4 have been used to suppress the backgrounds which contain jets. The signal and intrinsic backgrounds without jets ZZ, ZW, DY can also have some central jets from the intial state radiation radiation or from the pile up events. The jet reconstruction efficiency and the energy resolution drop rapidly with decreasing energy: for E_T^{jets} <20 GeV the efficiency is below 50% and the energy resolution degrades to $\sim 40\%$. Such jets have a large contamination from the calorimeter's noise, underlying events and pile up. Nevertheless they can be used to estimate the hadronic activity in an event.

The jets have been reconstructed in full and fast simulation from the calorimeter towers (ECAL+HCAL) with the iterative cone algorithm and with the seed energy $E_T^{seed} > 0.5$ GeV in the cone ΔR <0.5. The jets energy was calibrated using corrections from the γ-jet balancing [**?**]. The contamination of the jets at $|\eta|$ <1 from the noise was reduced by applying a threshold on the seed energy of the jets $E^{seed} > 0.8$ GeV. The jet was removed from the list if it matches within the $\Delta R < 0.3$ cone with a reconstructed electron. The E_T distributions of the jets for signal and some background channels is shown in Figure 6. The number of selected central jets with $E_T > 30$ GeV and $|\eta|$ <2.4 in signal and background data samples are shown on the right hand side of Figure 6.

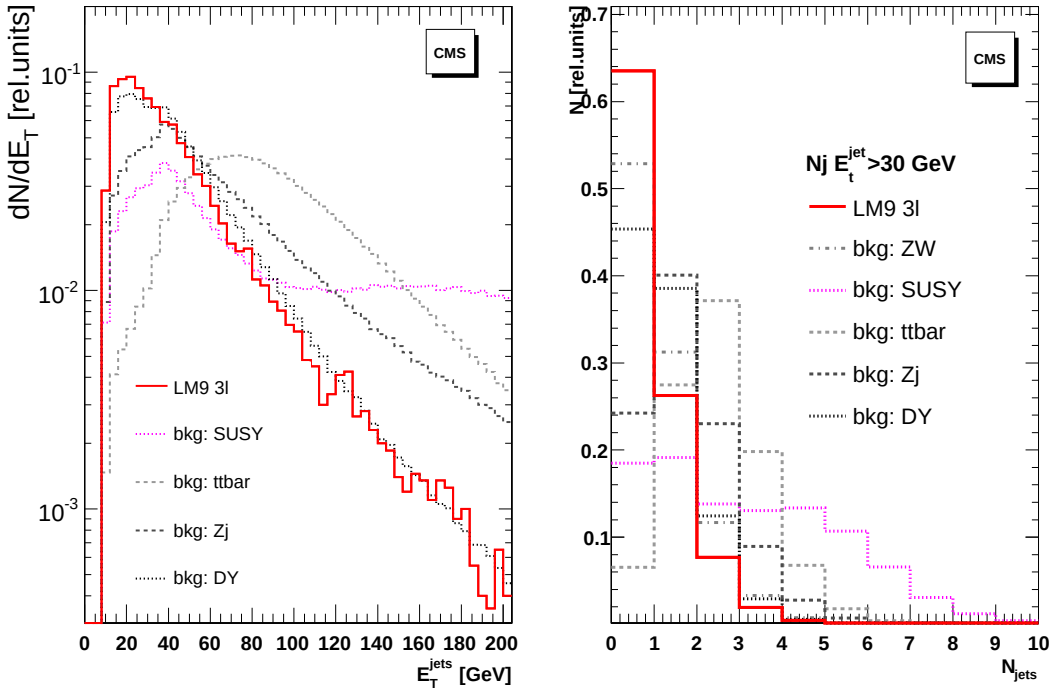

Figure 6: Normalized distribution of E_T^{jets} and number of jets per event with $E_T > 30GeV$ in the signal and background channels.

3.4 Missing transverse energy

In this study the Missing Transverse Energy (MET) was reconstructed from the HCAL plus ECAL towers and corrected for muon tracks. In an ideal detector the MET is almost zero for the leptonic decays (e, μ) in DY, Z + jets and ZZ backgrounds. The measured MET resolution for the considered channels is $\sigma_{MET} \sim \sqrt{\sum E_T} \sim 30$ GeV and it will increase the reconstructed MET. The MET calculated from MC particles and the reconstructed one are shown in Figure 7 for the signal and some backgrounds. Only $t\bar{t}$ and SUSY backgrounds have a distinct larger MET, the others are comparable with the signal. Hence, the use of this parameter in the event selection is not very efficient in contrast to other SUSY studies where the large MET is the main selection cut against SM backgrounds. The improvement of the MET reconstruction at low energy will allow a significant improvement of the suppression of Z+jets and DY background and is a subject for future study.

4 Event selection

The event selection and background suppression is done in two steps. In the first step, simple sequential cuts have been applied. In the second step the selected data samples have been used for a Neural Network (NN) training. The NN allows to combine various observables in one output and perform an optimized selection for each type of background. An advantage of the NN in comparison to the usual cuts is that the correlations between parameters are taken into account. The drawback of this method can be a somewhat larger sensitivity to the details of the simulation and larger samples are required for the training. Therefore the main background rejection was done with the sequential cuts. The effect of the NN selection is demonstrated for the LM9 point at large m_0, the low m_0 region would require another optimization.

4.1 Selection with the sequential cuts

The events have been selected using the following cuts:

- L1+HLT trigger

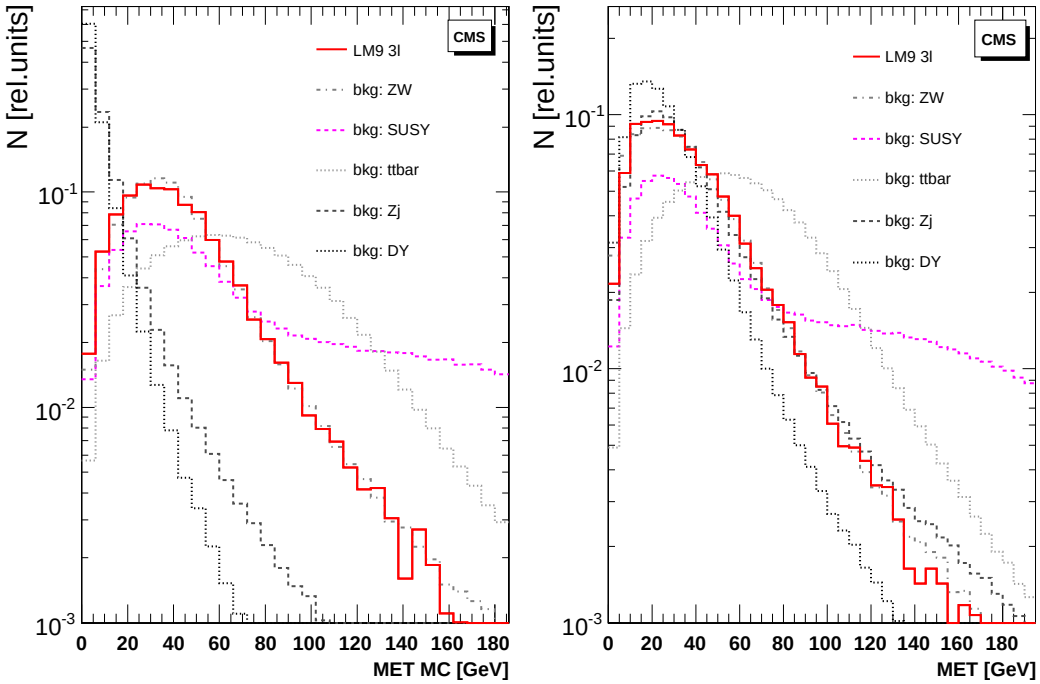

Figure 7: Normalized MET from MC particles and after reconstruction (FAMOS) for the signal and backgrounds.

- No jets with $E_T > 30$ GeV in $|\eta| < 2.4$.
- At least three isolated leptons in the acceptance of $|\eta| < 2.4$. Among them an OSSF pair of leptons with transverse momentum: P_T^{μ} >10 GeV/c and P_T^{e} >17 GeV/c and the invariant mass below the Z peak $M_{ll} <$ 75 GeV/c^2. The third lepton with $P_T^{\mu,e}$ >10 GeV/c.

The evolution of statistics and selection efficiencies with these selection cuts are shown in Table 6. The simulated statistics is scaled to 30 fb^{-1}. The requirement of three isolated leptons with two OSSF and $M_{ll} < 75$ GeV/c^2 is the most powerful selection against all backgrounds, the jets veto is important mostly for the $t\bar{t}$, QCD and SUSY. The largest contribution to the background after selection is coming from the DY, Z+jets, $t\bar{t}$ and ZW. For the W+jets and QCD backgrounds only a small part of the required statistics have been simulated ($\sim 10^6$), see Table 2, and no events have been selected. The upper limit on the expected number for the full data sample has been estimated using the probability to select 3 leptons at generator level and the selection cut efficiencies.

In case of trileptons of the same flavor or events with N_l >3 the dilepton invariant mass can be constructed from different OSSF combinations, for example the highest or lowest P_T pairs. The probability of correct pairing was analyzed at generator level and is almost the same for high or low P_T combinations. However the lowest P_T pairs are producing a lower invariant mass for the ZW, ZZ and Z+jets channels, thus moving the Z peak into the region of the signal and increasing the background.

The dilepton invariant mass distribution for high P_T pairs of the signal events is presented on Figure 8. The MC tagged OSSF pairs from the χ_2^0 decays are plotted for comparison. In $\sim 27\%$ of the signal events another OSSF pair can be constructed, with one lepton originating from the $\chi_1^{\pm}$ decay instead of χ_2^0 . Since $m_{\chi_2^0} \sim m_{\chi_1^{\pm}}$, however, this 'wrong' invariant mass stays in the considered region and the significance for all OSSF pairs is artificially enhanced. The invariant mass from all OSSF pairs is shown in Figure 9 (left) for signal and all backgrounds together with the different flavor opposite sign combinations $e^+\mu^- + e^-\mu^+$ (DFOS) which corresponds to the combinatorial background. The DFOS combinations have a maximum near the signal and its subtraction does not improve the significance for the LM9 point. The dielectrons contribute $\sim$25% to the signal as expected from the trigger selection. The S_{cp} significances [13] without systematic uncertainties at LM9 point for the high P_T and all OSSF combinations are 5.5 and 6.1 respectively. The kinematic end point M_{ll}^{max}=$m_{\chi_2^0} - m_{\chi_1^0}$ is largely deteriorated by the background and cannot be reconstructed at LM9 with a sufficient precision.

Table 6: Summary of the signal(LM1, LM9, LM7) and background statistics expected for $L_{int} = 30$ fb^{-1} at different selection steps. The selection efficiency with respect to the previous cut is shown in parentheses.

channel	N_{ev} (30fb^{-1})	L1	HLT	NoJets	$N^{l}_{rec} > 2$	$N_{isolated} > 2$ OSSF $M_{ll} < 75$GeV/c^2
LM1	2640	1795 (68%)	1544 (89%)	864 (56%)	337 (39%)	70 (21%)
LM7	1540	1360 (88%)	1250 (92%)	738 (59%)	310 (42%)	91 (29%)
LM9	3700	3182 (86%)	2896 (91%)	1740 (60%)	851 (49%)	238 (28%)
SUSY(LM9)	4 10^5	3.4 10^5 (85%)	2.5 10^5 (74%)	1.8 10^4 (7%)	1.4 10^4 (78%)	34 (0.24%)
ZW	5.10^4	3.98 10^4 (79%)	3.6 10^4 (92%)	1.9 10^4 (53%)	4900 (26%)	173 (3.5%)
ZZ	4800	3860 (80%)	3530 (91.5%)	1681 (48%)	818 (49%)	38 (4.6%)
$t\bar{t}$	2.6 10^6	2.1 10^6 (81%)	1.8 10^6 (86%)	1.3 10^5 (7%)	1.2 10^4 (9%)	239 (2%)
Z+jets(3l)	4.6 10^5	4. 10^5 (87%)	3.7 10^5 (92.5%)	9.8 10^4 (26.5%)	6.4 10^4 (65%)	504 (0.8%)
$Zb\bar{b}$	8.4 10^4	7.8 10^4 (93%)	7.3 10^4 (94%)	1.5 10^4 (20%)	1.1 10^4(73%)	69 (0.6%)
DY(3l)	4.5 10^5	3.6 10^5 (80%)	3.2 10^5 (89%)	1.4 10^5 (44%)	8. 10^4 (57%)	670 (0.9%)
Wt+jets	3. 10^5	2.7 10^5 (90%)	2.1 10^5 (78%)	3.9 10^4 (18.5%)	4910 (13%)	52 (1%)
WW+jets	6.10^5	4.5 10^5 (75%)	3.8 10^5 (84%)	1.9 10^4 (50%)	1.3 10^4 (68%)	7 (0.05%)
W+jets	5.4 10^8	1.9 10^8 (35%)	1.2 10^8 (68%)	7.8 10^7 (52%)	7.8 10^4 (0.1%)	0; < 94
QCD	7.4 10^{11}	3.3 10^{10} (4.5%)	6.6 10^8 (2%)	1.9 10^7 (3%)	1.9 10^3 (0.01%)	0; < 5

Among the selected trilepton events some reconstructed leptons are not traced back to the MC lepton at generator level. The tracing was done by matching reconstructed and generated MC lepton in the cone of $\Delta R < 0.2$. These events are considered as fakes. The rate of the fake events $F_{e,\mu}$ for the selected trileptons is presented in Table 7 for different backgrounds. For the electrons it is around $\sim 10^{-5}$ per selected trilepton event and for the muons $\sim 10^{-6}$. This includes leptons which appear at the reconstruction level, real leptons from $\pi^{\pm}, K^{\pm}$ decays, jets faking the leptons, and the mismatched leptons with large reconstruction errors.

The fakes leptons, especially electrons, will significantly increase background especially for the DY or Z+jets channels preselected at generator level. The number of fake events can be estimated from the probability to have a third fake reconstructed lepton(e or μ) in addition to the two real selected leptons. In this case the number of fake events for the full sample is: $N^{fake}_{e,\mu} = F_{e,\mu} * N_{tot} * E_{2l}$, where N_{tot} is the total number of events without preselection and E_{2l} is the efficiency to have two real reconstructed leptons passing the selection criteria. The efficiencies are estimated from the processed data samples. The expected number of fakes for different background channels is presented in Table 7. For the W+jets and QCD only an upper limit can be set. The fake leptons will increase the background for all trilepton combinations by $N^{fake}_{e,\mu}$=1053$\pm$166 events and, even more important, introduces large uncertainties in the background which decreases the signal significance. The muon fake rate is smaller (N^{fake}_{μ}=110$\pm$62) and the trimuon final state can be used as a discovery channel, see Figure 9(right). The significance with fakes included (without systematic uncertainties) for the trimuon state is S_{cp}=4.2 and 4.8 for all OSSF combinations.

Table 7: The estimated numbers of events containing a fake e or μ for different background channels at 30 fb^{-1}.

channel	N_{tot} 30fb^{-1}	F_e	F_μ	E_{2l}	N^{fake}_e	N^{fake}_μ
DY	$1.7 \cdot 10^9$	$2.6. \pm 0.5 \cdot 10^{-5}$	$4.3 \pm 2.5 \cdot 10^{-6}$	$1.8 \cdot 10^{-2}$	776 ± 163	127 ± 73
Z+jets	$3.4 \cdot 10^8$	$2.6 \pm 0.2 \cdot 10^{-5}$	$2.2 \pm 1.4 \cdot 10^{-6}$	$1.5 \cdot 10^{-2}$	133 ± 28	12 ± 8
ZW	$1.2 \cdot 10^6$	$6 \pm 4 \cdot 10^{-5}$	$< 10^{-5}$	$6 \cdot 10^{-3}$	< 0.3	< 0.1
ZZ	$6 \cdot 10^5$	$< 10^{-4}$	$< 10^{-4}$	$1.2 \cdot 10^{-2}$	< 0.5	< 0.5
$t\bar{t}$	$2.4 \cdot 10^7$	$4.6 \pm 1.8 \cdot 10^{-5}$	$< 10^{-6}$	$3.6 \cdot 10^{-2}$	3 ± 1	< 1
$Zb\bar{b}$	$4 \cdot 10^5$	$3 \pm 2 \cdot 10^{-5}$	$< 10^{-5}$	10^{-2}	< 0.5	< 0.5
Wt+jets	$1.7 \cdot 10^6$	$3 \pm 1.8 \cdot 10^{-5}$	$< 10^{-5}$	$5.3 \cdot 10^{-2}$	3 ± 1	< 1
W+jets($> 30 GeV/c$)	$5.4 \cdot 10^8$	$< 10^{-4}$	$< 10^{-5}$	$3.3 \cdot 10^{-4}$	< 18	< 1.8
QCD($> 50 GeV/c$)	$7.4 \cdot 10^{11}$	$< 10^{-4}$	$< 10^{-5}$	$1.7 \cdot 10^{-8}$	< 1.3	< 0.1

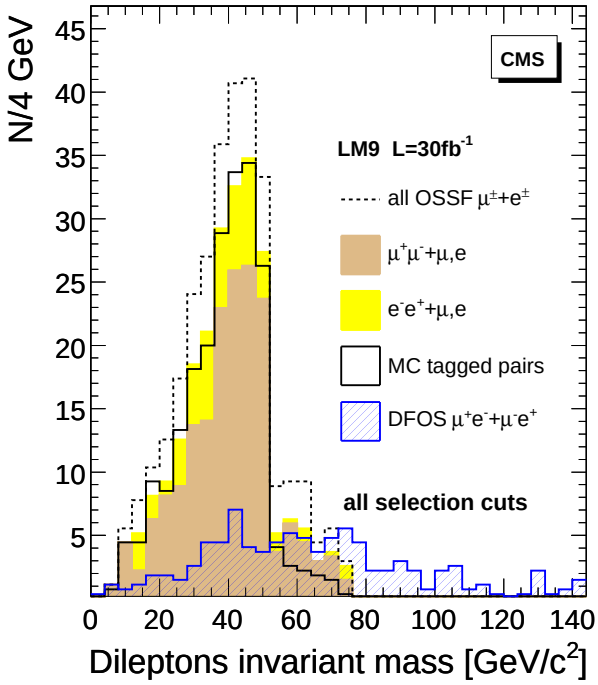

Figure 8: Reconstructed invariant mass distribution of the signal produced from the highest P_T dimuon or dielectron pairs, all OSSF pairs, DFOS and the MC tagged pairs.

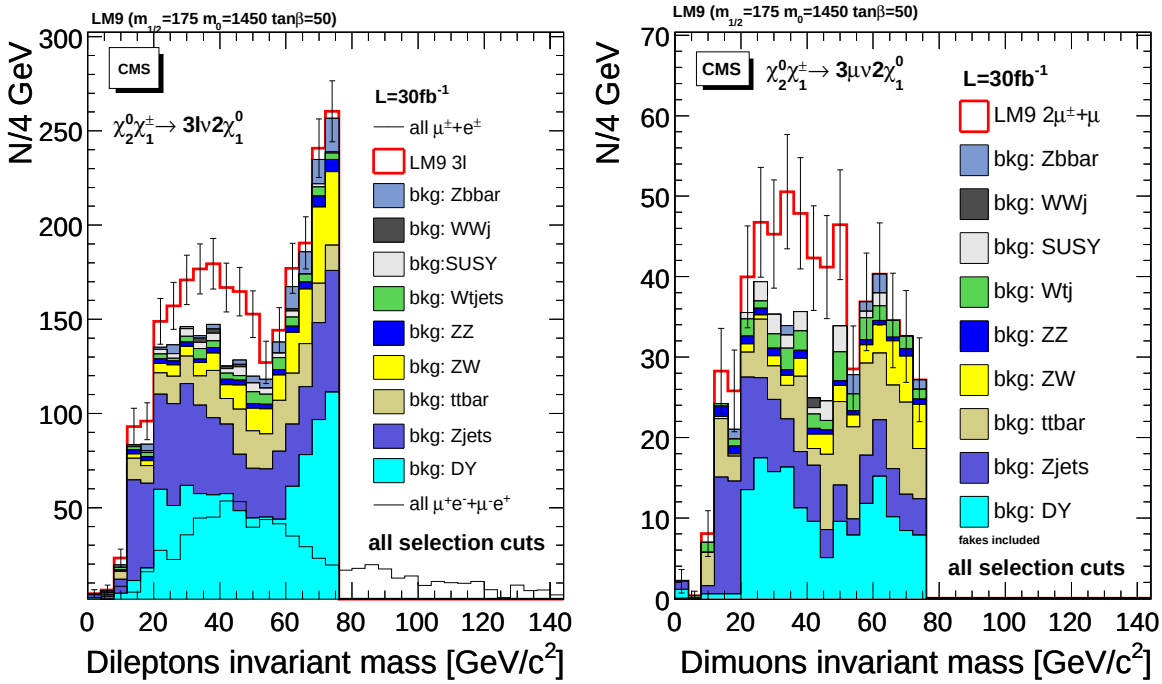

Figure 9: Left: Invariant mass for all OSSF combinations in each event for signal and backgrounds without fakes. Right: Invariant mass of the highest P_T trimuon combinations including the estimated fakes contribution.

4.2 Selection with the Neural Network

In this study the Neural Network software, available from [11], was incorporated into the analysis code. As an example, the reference LM9 point has been used for the network training. The following procedure has been implemented:

1. All data samples are split in two parts; training samples ($\sim 30\%$ of the statistics for each channel) with a priory knowledge of signal and background, and the main sample.
2. For each pair of signal-background a set of observables is defined.
3. The NN is trained separately for each signal-background pair using the training samples.
4. The selection cuts of the NN outputs were optimized simultaneously in order to get a maximum significance.
5. The main data samples are passed through the NN.

First of all the number of networks has to be defined. The important backgrounds with different topology found after selection with cuts (Z+jets, DY, $\mathrm{t\bar{t}}$, ZW and ZZ) have been used to build five networks. The data samples have been preselected. In order to increase the statistics somewhat looser selection cuts have been used for the training: $\mathrm{N}_{jets}(\mathrm{E}_T > 30$ GeV)< 2 and $\mathrm{P}_T^{\mu} > 5$ GeV/c, $\mathrm{P}_T^{e} > 10$ GeV/c. The size of each training sample was 3000 events for signal and background. This statistics was considered sufficient since smaller samples ($\sim$1000 events) produced similar results.

The trilepton final state has a rather limited number of observables which can be used for selection. The main observables are related to the lepton kinematics. All observables can be divided into different categories:

- Leptons related:
  $\mathrm{P}_T^{1,2,3}$ - transverse momentum and η - rapidity of three leptons ordered by P_T, $\mathrm{M}_{\mathrm{inv}}^{h,\ell}$ (invariant mass of high and low P_T OSSF pair combination), $\sum \mathrm{P_T}$ (sum of P_T of all leptons in the event), $\sum \mathrm{E}^{\ell}$ (sum of the energy of all leptons in the event), $A = \frac{\mathrm{P_T^1} - \mathrm{P_T^2}}{\mathrm{P_T^1} + \mathrm{P_T^2}}$ (asymmetry of the OSSF leptons), $\Theta_{\ell\ell}$ (angle between the two OSSF leptons), $\Theta_{\ell 1 \ell 3}$ (angle between the highest and lowest P_T leptons), $\Phi_{\ell\ell}$ (angle in transverse plane between two OSSF leptons), $\mathrm{P_T^{2\ell}}$ (transverse momentum of two OSSF leptons), N_{ℓ} (number of selected leptons).
- Energy balance variables:
  MET, $\sum E_T$ (reconstructed MET and sum of E_T in an event), $\Theta(\mathrm{MET}, \mathrm{P}_{2\ell})$ (angle between MET and OSSF lepton pair), MET + $\sum \mathrm{P_T}$.
- Jets related:
  Here the jets with too small E_T ($\mathrm{E}_T < 30$ GeV) or too big rapidity ($|\eta| > 2.4$), which cannot veto the event, have been used. N_{jets} (number of jets), E_t^{hj} (of the highest E_T jet), η_{hj} (rapidity of the highest E_T jet).

The variables are automatically sorted according to the significance by the NN and the redundant ones are removed. A summary of the variables used in the training is presented in Table 8. The distribution of NN outputs after training for different signal-backgrounds are shown in Figure 10. The lines show the signal efficiency and background contamination.

Table 8: NN variables for five neural networks used in analysis.

NN	NN variables
Z+ jets	P_T^3, M_{inv}^h, η_j, MET, Θ_{ll}, $\sum P_T$
DY	P_T^3, P_T^{2l}, $\sum P_T$, Θ_{ll}, MET, Φ_{ll}
$\mathrm{t\bar{t}}$	MET, $\sum P_T$, P_T^3, Θ_{ll}, E_T^{hj}, P_T^2, M_{inv}^h, P_T^1
ZW	$\sum P_T$, P_T^2, M_{inv}^h, M_{inv}^l, $\sum E^l$, Θ_{ll}, Φ_{ll}, A
ZZ	$\sum P_T$, MET, P_T^2, M_{inv}^h, Θ_{ll}, P_T^3,Φ_{ll}, A

The selection cuts on the NN outputs have been optimized using the Genetic Algorithm (GARCON) [12]. First the main data samples have been preselected using the selection cuts defined in the Section 4.1. It was found that

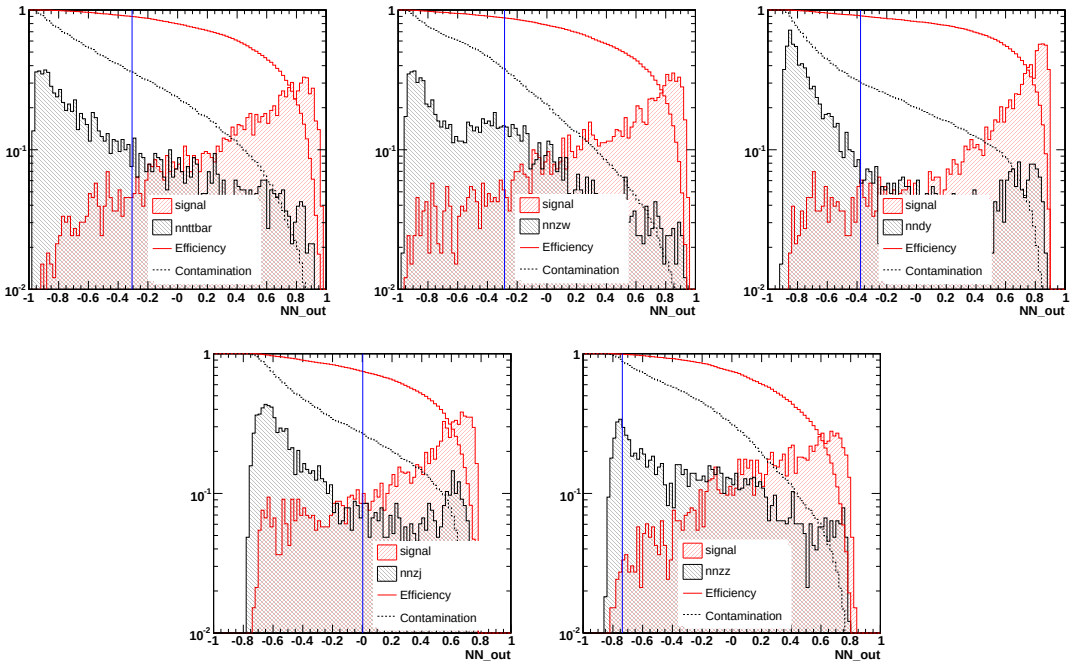

Figure 10: NN outputs for different signal-background pairs after training. The selection cuts optimized with Genetic Algorithm are shown as a vertical line. The efficiency and contamination are plotted as curved lines.

such a preselection gives a better significance than using the looser cuts used for the training samples. It means that the NN selection was less effective for the low P_T leptons as compared with the cuts. The selected events have been passed through different NNs and the five NN outputs for each event were used as input for the GARCON optimization with each input weighted with the cross section of the background signature. The GARCON defines all possible combination of NN cuts in steps of 2.5% of the scale and maximizes the significance S_{cL}. The obtained set of NN cuts for the final selection is shown in Figure 10. The efficiencies of the optimized NN selection cuts are presented in Table 9. The efficiency of each individual network was evaluated by enabling only one network at once. The NN$_{all}$ corresponds to the final selection when all networks have been activated. The final efficiencies of the signal and backgrounds separation are 68% and 26% respectively. The invariant mass distributions after NN selection of all OSSF combinations is shown in Figure 11 (left). The NN selection improves the significance for all OSSF pairs (no fakes) from S_{cp}=6.1 for the analysis with sequential cuts to 7.8 for the NN. The fakes contribute 221$\pm$48 events to the total trilepton sample and 31$\pm$16 to the trimuons. The invariant mass for the trimuon state with the fakes is shown on the right hand side of Figure 11 (right). The significance (without systematic uncertainties) is S_{cp}=5.1 for the trimuons with fakes and and 6.5 for all OSSF combinations.

The stability of the NN selection can be verified by using NNs trained with another signal. The training and the cut optimization have been repeated for the LM7 test point and the produced networks have been used for the LM9 selection. The cuts changes the interplay between different backgrounds however the S_{cp} significance for the LM9 test point selected with the LM7 networks is decreased only from 7.8 to 7.5.

5 Significance and systematic uncertainties

The significance was calculated using definitions from [13], where the S_{cp} significance is defined as a probability to observe signal over the Poisson distributed background and can take into account systematic and statistical uncertainties. There are several sources of uncertainties which will degrade the significance.

- Reconstruction and selection uncertainties. The number of selected events is sensitive to the reconstruction uncertainties in the leptons momentum, jets energy and MET calculations. These uncertainties have two components; the energy scale which shifts jets E$_T$, MET and P$^{e,\mu}$ for all events, and the resolution which smears the measured values event by event. The effect of these uncertainties on the number of selected events was evaluated by shifting and smearing the reconstructed quantities while using the same selection

Table 9: Selection efficiencies with the neural networks trained for the LM9 point. The individual NN efficiencies E(NN_i) correspond to the particular network enabled.

channel	N_{ev}, 30fb^{-1}	E(cuts) (N_{sel})	E(NN_{zw})	E(NN_{zz})	E(NN_{ttbar})	E(NN_{zj})	E(NN_{dy})	E(NN_{all}) (N_{sel})
LM1	2640	2.7% (70)	87%	72%	76%	52%	93%	24% (17)
LM7	1540	5.9% (91)	91%	87%	95%	81%	98%	62% (57)
LM9	3700	6.4% (238)	92%	92%	97%	81%	97.5%	68% (161)
SUSY	4 10^5	0.009% (34)	76%	85%	65%	95%	98%	65% (22)
ZW	5.10^4	0.3% (173)	65%	44%	86%	86%	97%	23% (44)
ZZ	4800	0.8% (38)	74%	60%	91%	81%	95%	39% (15)
$t\bar{t}$	2.6 10^6	0.01% (239)	76%	78%	65%	77%	98%	37% (89)
Z+j(3l)	4.6 10^5	0.1% (504)	81%	88%	94%	43%	88%	26% (129)
$Zb\bar{b}$	8.4 10^4	0.08% (69)	84%	90%	93%	42%	86%	26% (18)
DY(3l)	4.5 10^5	0.15% (670)	90%	85%	94%	30%	77%	19.5% (131)
Wt+jets	3.10^5	0.017% (52)	74%	74%	73%	71%	99%	38% (20)
WWj	6.10^5	0.001% (7)	83%	83%	67%	67%	100%	29% (2)
Tot.bkg	4.9 10^6	0.035% (1786)						26% (470)

procedure. For the integrated luminosity above 10 fb^{-1} the energy scale uncertainty is expected below $\delta_{jes} = 5\%$ and the energy resolution $\sigma_j = 5\%$. The MET and jets E_T are assumed to be correlated: E_T^j= Gauss(E_T^j, σ_j)* (1+δ_{jeS}), MET=MET-$\sum \Delta E_T^j$. The muon(electron) momentum scale uncertainty is $\delta_p = 1\%(2\%)$ and the resolution $\sigma_j = 1\%(2\%)$ as well. After selection with cuts the number of background events is changed by 3.3%, moslty due to jets energy scale errors. For the NN where more parameters were used, the effect of the jet energy scale and resolution errors is smaller $\Delta N_b = 1\%$. Even doubling the errors ($\delta_{jes} = 10\%$, $\delta_p = 5\%$) increases the ΔN_b to 1.2% only.

- PDF uncertainties. For the estimation of the PDF uncertainties the CTEQ6i set comprised of 41 subsets was used from the LHPDF library [14]. The uncertainties have been estimated using the PDF reweighting technique. For each event a vector of weights for each i subset was calculated as: $w_i = \frac{PDF_i(x_1,x_2,Q)}{PDF_0(x_1,x_2,Q)}$, where $x_{1,2} = p_L/s$ are the Bjorken variables of the partons (q, g) participating in the hard process, Q=$s\sqrt{x_1 x_2}$ is the energy scale of the event, PDF_i and PDF_0 are the tested and the reference PDF subset. The reweighting was implemented in the analysis code and the PDF uncertainties are calculated for the signal and backgrounds. The normalized number of selected events N=$\sum w_i$ for different channels is plotted in Figure 12. The background samples have been weighted according to the selection efficiencies. The total sigma of the background distribution is $\sigma = 1.73\%$. The σ_{PDF} and the max-min spread of the event distribution $\frac{N_{PDFi}}{N_{PDF0}}$ are listed in Table 10.

Table 10: Systematic uncertainties of the LM9 signal and backgrounds.

channel	PDF $\sigma_{\frac{Npdfi}{Npdfo}}$, (min, max), %
LM9 3l	1.2 (-3.0 +2.5)
ZW	1.2 (-3.0 +2.2)
ZZ	1.3 (-3.4 +2.4)
$t\bar{t}$	0.9 (-3.5 +3.2)
Wt+jets	1.2 (-4.5 +4.2)
SUSY	1.2 (-4.0 +4.2)
$Zb\bar{b}$	1.4 (-5.0 +3.7)
DY	2.1 (-6.2 +6.3)
Z+ jets	1.6 (-5.5 +3.7)
Tot.weighted %	1.72

The reconstruction errors and the theoretical systematic together contribute only $\sim 2\%$ to the background uncertainties. These uncertainties reduce the significance to 4.8 for the trimuons and to 5.8 for all OSSF combinations. However the dominant contribution is coming from the statistical errors in the fake rates estimation, which in-

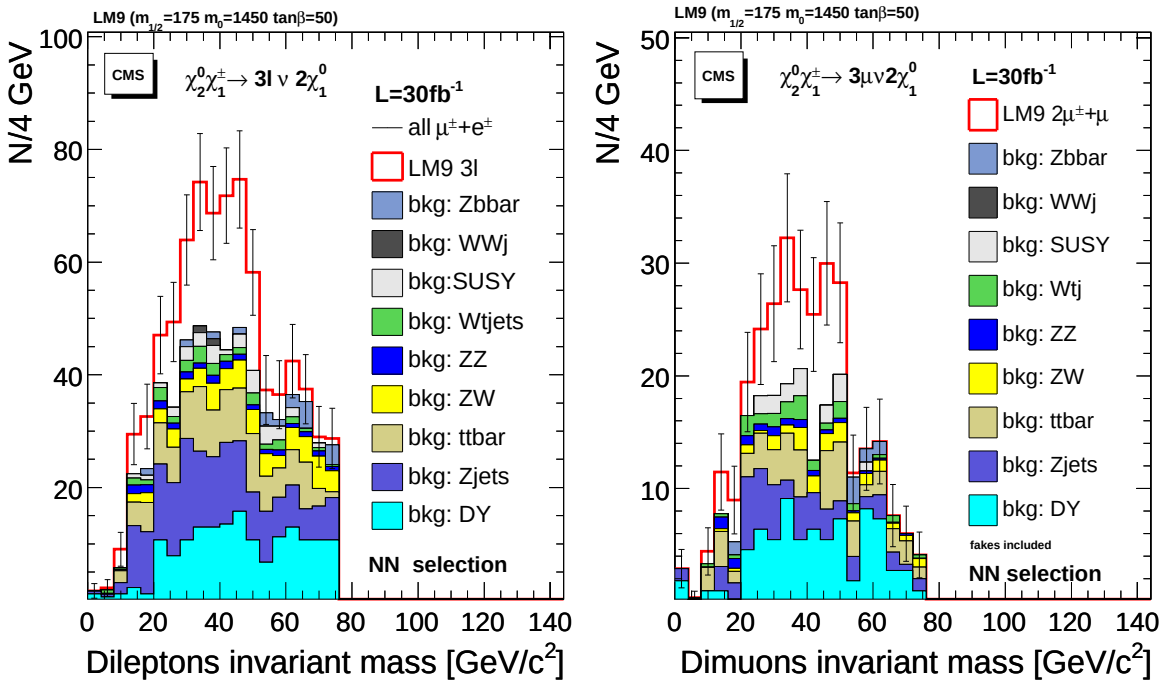

Figure 11: Left: Invariant mass distribution of all OSSF lepton combinations after selection with the NN trained for the LM9 benchmark point without fakes. Right: Invariant mass for the high P_T dimuon combinations in the trimuon final state with the fakes included.

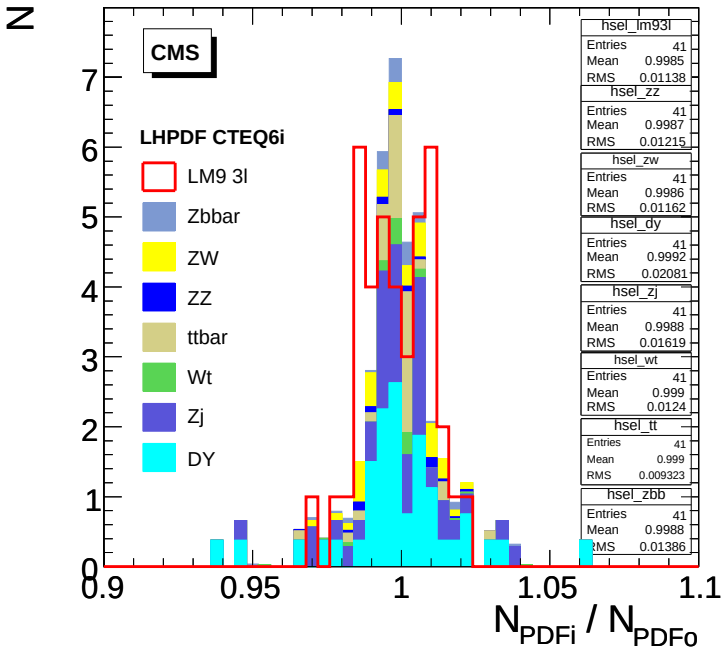

Figure 12: Distribution of the selected events with different reweighted CTEQ6i PDF subsets for the signal and backgrounds normalized according to the selection efficiencies.

creases the background uncertainties to $\sim$ 7% and decreases the significance to 3.3 for trimuons and 3.2 for all OSSF. This uncertainty in the fake rates can be reduced with larger simulated samples and further optimization of the leptons reconstruction. In this estimate the theoretical uncertainties from the cross section and QCD effects are not taken into account since they will be studied in the first years of LHC operation.

6 CMS discovery reach

For the CMS discovery reach, the m_0, $m_{1/2}$ mSUGRA plane was scanned with FAMOS for two values of tanβ (tanβ=10,50) and $m_{1/2} > 140$ GeV. The S_{cp} significance contours obtained with the the NN selection for all OSSF combinations and the trimuon final state are shown in Figure 13 for $L_{int} = 30$ fb^{-1}. The systematic uncertainties coming from reconstruction and PDF are included. The discovery reach with the statistical uncertainties in the fake rates is shown for the trimuon final state. Among the CMS test points only LM9 can be marginally seen and the discovery reach is limited by a low value of $m_{1/2}$ <180 GeV. The two body decay region at low $m_0 < 100$ GeV is visible for tanβ=10 even with the selection optimized for the three body decays at large m_0. In this region the MET has a long tail and the MET cut can be used for the background suppression. Further improvement of the NN selection is possible with the training performed for each region in m_0,$m_{1/2}$ plane.

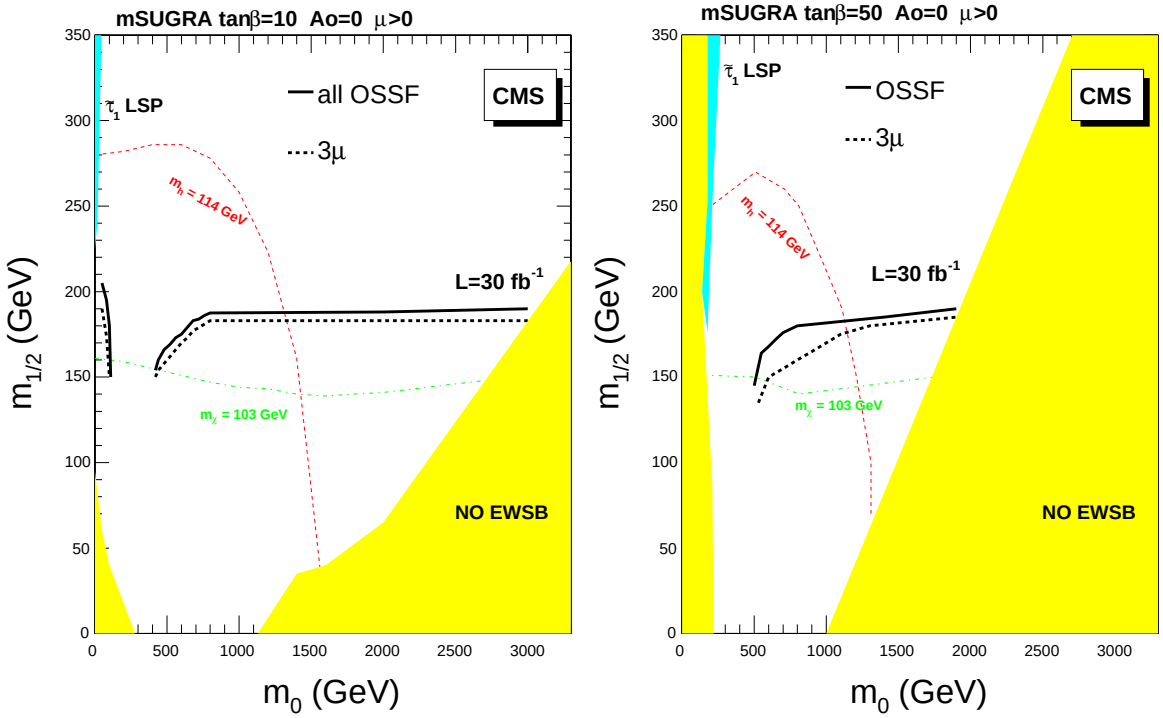

Figure 13: The CMS 5 σ discovery reach plot at 30fb^{-1} for the all OSSF pairs(dashed) in trilepton final state and for trimuons(solid) with the reconstruction and theoretical systematics uncertainties.

7 Conclusion

The direct neutralino-chargino $\chi_2^0\chi_1^\pm$ production with the trilepton final state has been studied in presence of the most important backgrounds with a realistic CMS simulation. The trilepton events can be selected with a central jets veto and by requiring OSSF leptons with invariant mass <75 GeV/c^2. The selection with a neural network improves the significance from 6.1 to 7.8 for the LM9 point ($m_{1/2}$=175, m_0=1450, tanβ=50). The 5σ signal can be observed in dilepton invariant mass at large $m_0 > 1000$ GeV for an integrated luminosity of 30fb^{-1} for low $m_{1/2} < 180$ GeV. The main background is coming from the DY, Z+jets and $t\bar{t}$ channels and the fake leptons have an important contribution. The suppression of these backgrounds is difficult due to the small missing transverse energy in the signal events which makes the discovery of the mSUGRA trilepton at CMS challenging. At high luminosity the selection would require another optimization due to a larger rate of pile up events which will decrease the efficiency of the jets veto.

The SUSY exclusive trilepton channel is complementary to the inclusive dilepton search which potentially has larger significance. The simultaneous observation of both signatures will be an independent check of the neutralino decays and will identify a region in mSUGRA parameter space.

8 Acknowledgments

We would like to thank L. Pape, M. Spiropulu, S. Abdullin, F. Moortgat, M. Chiorbioli, M. Galanti, M. Chertok, L. Dudko, S. Bityukov for useful discussions. We also thank G.Quast and Karlsruhe production team for the help in simulations.

References

[1] A.Canapa, E.Lytken. CDF NOTE-7833 (2005).

[2] W. de Boer et al., AA, 444, 51 (2005).

[3] T. Sjostrand et al. [arXiv:hep-ph/0603175], (2006).

[4] F. Paige et al. [arXiv:hep-ph/0312045], (2003).

[5] CMS PTDR Vol.1.CERN-LHCC-2006/001. (2006).

[6] LEPHIGGSWG, CERN-EP/2003-011 (2003), ALEPH, Phys.Lett.B583 (2004).

[7] W. Beenakker et al., [arXiv:hep-ph/9906298], (1999).

[8] S. Slabospitsky, l. Sonnenschein, [arXiv:hep-ph/0201292], (2002).

[9] M. Mangano et al. [arXiv:hep-ph/0206293], (2002).

[10] S. Baffioni et al. CMS-NOTE 2006/040. (2006)

[11] M. Feindt. [arXiv:physics/0402093] .

[12] .S. Abdullin et al. [arXiv:hep-ph/0605143].

[13] S. Bityukov, N. Krasnikov. CMS-CR 2002/005 (2002).

[14] LHPDF ($\mathrm{http://hepforge.cedar.ac.uk/lhapdf}$).